Available online at www.sciencedirect.com

ScienceDirect

Ceramics International 40 (2014) 2209–2220

CERAMICS INTERNATIONAL

www.elsevier.com/locate/ceramint

Effect of polyethylene glycol on porous transparent TiO_2 films prepared by sol–gel method

J.M. Calderon-Moreno[a], S. Preda[a], L. Predoana[a], M. Zaharescu[a], M. Anastasescu[a,*], M. Nicolescu[a], M. Stoica[a], H. Stroescu[a], M. Gartner[a], O. Buiu[b], M. Mihaila[b], B. Serban[b]

[a]*Institute of Physical Chemistry "Ilie Murgulescu", Romanian Academy, Spl. Independentei 202, 060021 Bucharest, Romania*
[b]*Honeywell Romania SRL, Calea Floreasca Nr. 169A, 014459 Bucharest, Romania*

Received 7 June 2013; received in revised form 16 July 2013; accepted 29 July 2013
Available online 3 August 2013

Abstract

Multilayered titania (TiO_2) films have been prepared via sol–gel dip-coating method from a tetraethyl-orthotitanate solution that contains 2 g of polyethylene glycol (PEG) with different molecular weight (6000, 20,000 and 35,000). The films were deposited on fluorine doped tin oxide (FTO) coated glass and annealed by a thermal treatment at 450 °C for 30 min. We demonstrated how the structure, the morphology and the optical properties of the films can be controlled by varying the PEG molecular weight and number of depositions. The correlation between these parameters and the film properties was investigated. Sol–gel deposited and PEG doped TiO_2 films demonstrate better properties for their use in solar cell applications, by enhancing the transmittance value in the 380–540 nm range.

Keywords: B. Electron microscopy; C. Optical properties; Sol–gel method; PEG doped TiO_2

1. Introduction

Titanium dioxide thin films are of great interest for their application in solar cells [1–4], gas and humidity sensors [5], catalyst supports [6–8], construction of optical wave-guides [9–10], thin film capacitors [11,12], and inorganic membranes [13,14] as well as electrochromic materials [15,16]. For new devices in chromatography [17–19] or dye-sensitized solar cells [20–23], it is essential to obtain thin porous films with well controlled size and pore distribution.

TiO_2 films have been prepared by various methods, either physical or chemical; as for physical methods, results on ultrasonic spray pyrolysis [24], magnetron sputtering [25] and pulse laser deposition (PLD) [26] were reported. Thin and thick films obtained by various chemical methods such as – chemical spray pyrolysis [27], chemical vapor deposition (CVD) [28] and the sol–gel method [29–33] were successfully achieved. Films with predetermined morphology can be synthesized using the sol–gel methods by changing the solution composition and deposition conditions. Previous results concerning the sol–gel preparation of TiO_2 films with anatase structure, in the presence of PEG, were reported by Bu et al. [34]. The $Ti(OC_4H_9)_4$ has been used as TiO_2 source in the presence of PEG with 800, 1000 and 2000 molecular weight and different complexing agents. Similar TiO_2 precursor was used by Gartner et al. [35] to prepare TiO_2 doped films and also by Sun et al. [28] using PEG with molecular weight of 400, 2000, 6000 and 22,000.

Porous films have been obtained by using PEG as a chelating agent. Trapalis et al. [6] used PEG in order to control the porosity of Fe^{3+} doped TiO_2 films starting with $Ti(OC_2H_5)_4$ as TiO_2 precursor and PEG with molecular weight of 600. The porosity increases with the PEG amount introduced in the film.

Sonawane et al. [36], Liau et al. [8] and Guo et al. [29] prepared TiO_2 films starting with $Ti(OC_3H_7)_4$ and PEG with different molecular weights and amounts. The amount of PEG used in the papers mentioned above varied between 1 and 9%.

The present study reports on the effects of PEG – with different molecular weights – on the structural, morphological and optical properties of TiO_2 thin films derived from sol–gel technique. Porous TiO_2 films were synthesized using the sol–gel dip-coating method from an alkoxide-based solution that contains PEG.

*Corresponding author. Tel.: +40 213 167 912; fax: +40 213 121 147.
E-mail address: manastasescu@icf.ro (M. Anastasescu).

0272-8842/$ - see front matter © 2013 Elsevier Ltd and Techna Group S.r.l. All rights reserved.
http://dx.doi.org/10.1016/j.ceramint.2013.07.139

Table 1
Composition of solution and experimental conditions of sol preparation.

Reagents	Molar ratio			pH sol	Experimental conditions	
	$\frac{R^aOH}{\sum precursor}$	$\frac{H_2O}{\sum precursor}$	$\frac{catalyst}{\sum precursor}$		T (°C)	t (h)
$Ti(OC_2H_5)_4$ PEG	36.5	1.35	0.35	3	Room temperature	2

[a]$R = -C_2H_5$.

Table 2
The variation of viscosity versus PEG molecular weight.

Sample (Sol)	Viscosities (cP)
TiO_2	2.00
TiO_2 with PEG 6000	2.04
TiO_2 with PEG 20,000	2.10
TiO_2 with PEG 35,000	2.40

The synthesized films were characterized using X-Ray diffraction (XRD), scanning electron microscopy (SEM), atomic force microscopy (AFM), and spectroellipsometry (SE).

The correlation between the main technological parameters and the materials properties was investigated towards the use of the films for solar cell, photocatalysts and porous matrix applications.

2. Experimental

2.1. Film deposition

The composition of the initial solution and the experimental conditions for obtaining sol–gel oxide films in the above mentioned system are presented in Table 1.

Tetraethyl-orthotitanate $Ti(OC_2H_5)_4$ (Merck) was used as TiO_2 source. Ethanol was used as solvent, nitric acid as catalyst and water for hydrolysis. The molar ratio of the reagents presented in Table 1 has been selected based on the previous work [32] that has established the experimental

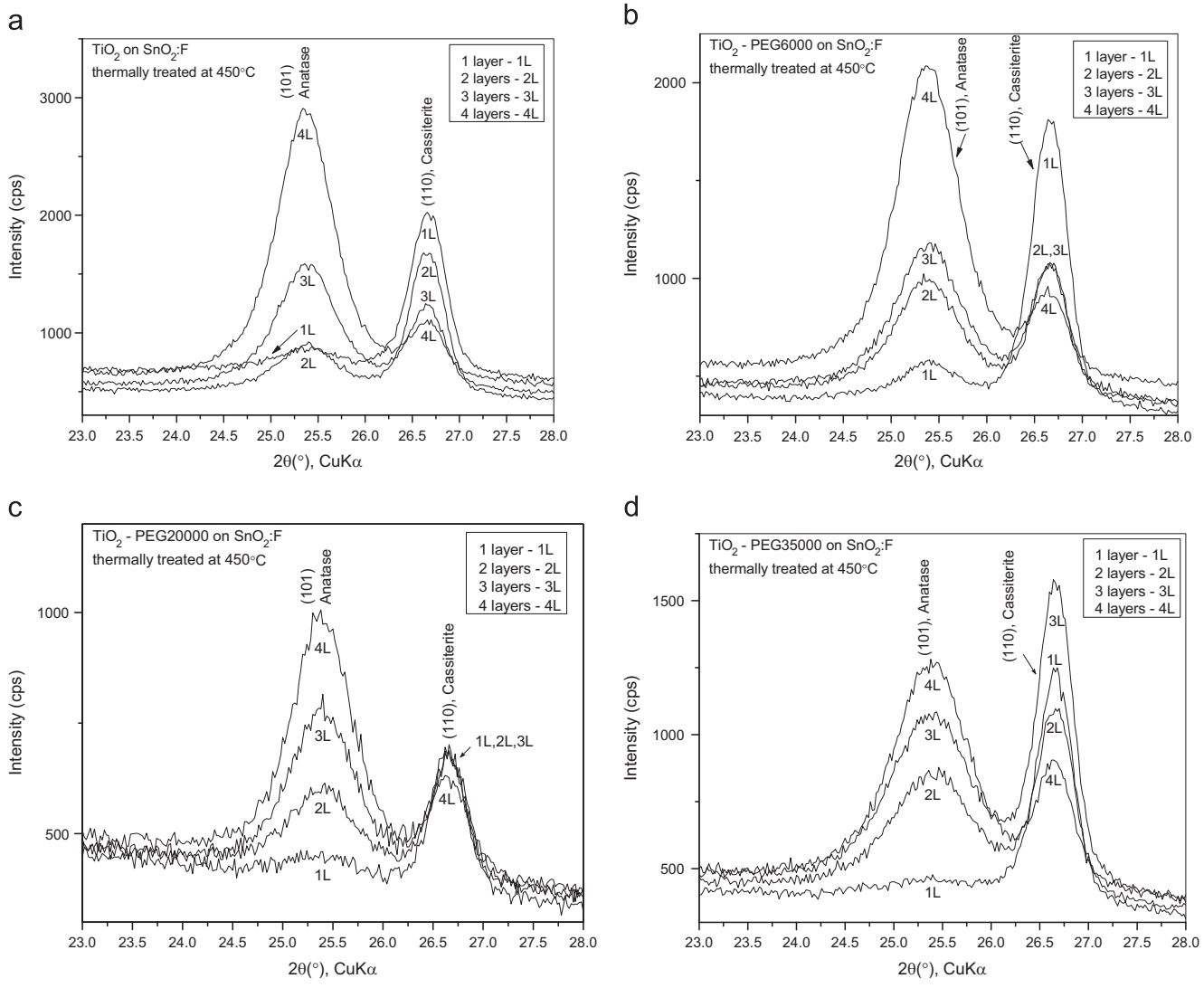

Fig. 1. XRD patterns, in the region of anatase 101 peak, of 1–4 layers TiO_2 films, treated at 450 °C, doped with PEG of different molecular weight: (a) without PEG; (b) PEG, molecular weight 6000; (c) PEG, molecular weight 20,000 and (d) PEG, molecular weight 35,000.

conditions to prepare stable solutions that allow multilayers depositions. The results were applied to successfully prepare pure [33] and doped TiO_2 films [37–39]. Based on the literature data [6,8,28,29], PEG with molecular weights of 6000, 20,000 and 35,000 were chosen and a concentration of the solutions of 2 g PEG to 1 mol $Ti(OC_2H_5)_4$. The reaction was kept under stirring at room temperature for 2 h.

From these solutions, films were deposited on TCO30-8 (3 mm thick soda lime glass coated on one side with a fluorine doped tin oxide (SnO_2:F) layer) substrate (further denoted as the FTO glass) by the dip-coating method at a withdrawal rate of 5 cm/min. Before deposition, the solutions were aged for 24 h. A thermal treatment (TT) at 450 °C for 30 min, using a heating rate of 5 °C/min was applied to the films; for multilayer films, a TT of densification (300 °C for 30 min, with a heating rate of 5 °C/min), was used after each layer deposition.

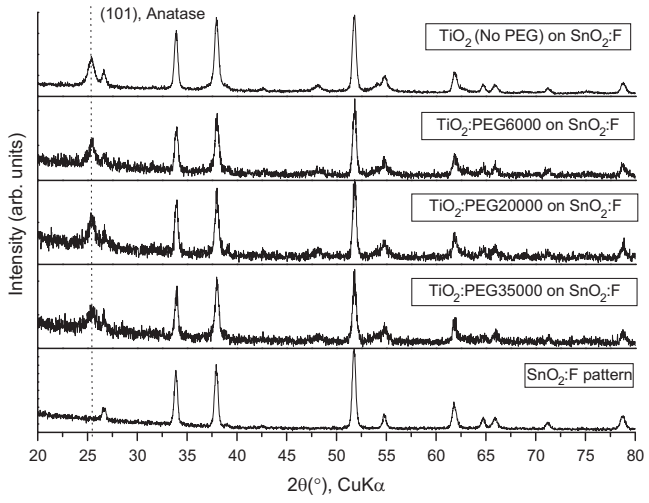

Fig. 2. XRD patterns of the substrate and 4 layer films, with different PEG molecular weights.

The viscosities of the solutions were measured at room temperature before deposition with Brookfield Viscometer DV-II+Pro equipment in 8 ml of solution and the data are presented in Table 2. The viscosity of the prepared solutions increased when PEG with higher molecular weight was used.

2.2. Film characterization

PEG doped and undoped TiO_2 films were characterized structurally through XRD, morphologically by SEM and AFM, as well as optically by SE.

The XRD measurements were performed using an Ultima IV X-Ray Diffractometer (Rigaku, Japan) using Cu Kα radiation (Kα = 1.54056 Å) at an accelerating voltage of 40 kV and a current of 30 mA. For thin films, the diffractometer was set in condition of grazing incidence X-ray diffraction (GIXD), with $\omega = 0.5°$. The samples were scanned in the range from 20° to 90° of 2θ with a scan rate of 5°/min, continuous scanning, and from 23° to 28° of 2θ with a fixed time of 4 s/0.02°.

Systematic information on the thin film morphology was obtained by SEM using a FEI Quanta 3D microscope operating at 20 kV, coupled with energy dispersive X-ray (EDX) spectroscopy measurements.

AFM measurements were carried in the non-contact mode, with a XE-100 apparatus from Park Systems (2011), using sharp tips (< 8 nm tip radius; PPP-NCHR type from Nanosensors™). The topographical 2D and 3D AFM images were taken over the area of $8 \times 8\ \mu m^2$ area; for displaying purpose and subsequent statistical data analysis (including the calculation of the root mean square (RMS) roughness) it was used the XEI (v.1.8.0) Image Processing Program developed by Park Systems.

Table 3
Anatase (101) diffraction line position (2θ), interplanar spacing (d_{hkl}), the full-width at half-maximum (FWHM) and the crystallite size of TiO_2 films, annealed at 450 °C.

Molecular weight of PEG	Layer numbers	2θ (°)	d_{hkl} (nm)	FWHM (°)	Crystallite size[a] (nm)
0	1	25.371	0.350	0.9375	9.07
	2	25.374	0.350	0.7634	11.14
	3	25.369	0.350	0.7435	11.43
	4	25.348	0.351	0.7138	11.91
6000	1	25.342	0.351	0.7908	10.75
	2	25.355	0.350	0.8175	10.40
	3	25.377	0.350	0.8414	10.10
	4	25.348	0.351	0.7657	11.10
20,000	1	25.423	0.350	0.8199	10.37
	2	25.412	0.350	0.7847	10.84
	3	25.378	0.350	0.7685	11.06
	4	25.362	0.350	0.7176	11.85
35,000	1	25.347	0.351	1.7415	4.88
	2	25.409	0.350	1.0667	7.97
	3	25.379	0.350	1.0184	8.35
	4	25.369	0.350	0.9345	9.10

[a]The crystallite size was determined using Scherer's formula only for (101) diffraction line of anatase.

Table 4
Unit cell parameters of anatase, TiO_2, calculated for 4 layers film in comparison with the standard values.

PEG molecular weight in the samples	a (nm)	b (nm)	c (nm)	α (°)	β (°)	γ (°)
0	0.3815(3)	0.3815(3)	0.95158(13)	90	90	90
6000	0.3808(4)	0.3808(4)	0.95139(19)	90	90	90
20,000	0.3827(4)	0.3827(4)	0.9546(3)	90	90	90
35,000	0.3898(5)	0.3898(5)	0.9565(5)	90	90	90
TiO_2, anatase, ICDD file no. 01-089-4203	0.37850	0.37850	0.95140	90	90	90

SE measurements were performed with a VASE ellipsometer for UV–vis–NIR range from Woollam Co., Inc. Measurements have been performed at the 70° incidence angle and a 5 nm step in air at room temperature.

3. Results

3.1. XRD

Measurements were performed in the 20–80° range, with a more detailed analysis in the 23–28° (2θ) domain. The domain for a more detailed investigation was selected because of the presence – at $2\theta = 25.30°$ – of the most intense diffraction line for TiO_2 anatase (101), according to ICDD file no. 01-089-4203. In the same range the FTO glass substrate presents also a diffraction line at $2\theta = 26.611°$ assigned to SnO_2 cassiterite (110) line, according to ICDD file no. 00-041-1445.

The results are presented in Fig. 1(a–d).

It can be noticed that the intensity of the anatase (101) peak increases with the number of deposited layers and also with the subsequent TT at 450 °C, due to a better crystallization of the resulting coatings. At the same time the intensity of the SnO_2 (110) diffraction line from the substrate decreased.

Other diffraction lines of crystalline TiO_2 anatase phase, except (101), cannot be evidenced because they superpose with the diffraction lines of SnO_2 (Fig. 2). The (101) diffraction line of anatase at $2\theta \sim 25°$ appears from the first deposition layer in all cases (Fig. 1), so we can conclude that the films are crystalline after the first deposition, which is in good agreement with SEM observations (see below).

Making a comparison between the XRD patterns of the samples with 4-deposited layers (Fig. 2), it can be seen that the diffraction lines widen with increasing PEG molecular weight, indicating that nanocrystallite size decreases, as confirmed also from the calculation of crystallite sizes based on Scherrer's formula (results presented in Table 3).

One can notice that the unit cell parameters of the anatase crystals are larger than indexed ones. It can be easily observed from the X-ray patterns that the shape, intensity and FWHM of the diffraction lines is not representative for well-crystallized, but for nanosized, poorly crystallized materials. The unit cell parameters of anatase of the sample containing PEG 6000 is the closest to indexed parameters. The crystallite size for this sample is 11.10 nm. On the other side, the unit cell parameters of anatase of the sample containing PEG 35,000 with the largest molecular weight have the smallest crystallite size (9.1 nm). The higher the molecular weight of PEG, the higher is the influence on the unit cell parameters of anatase. The unit cell parameters (Table 4) were calculated, using PDXL software from Rigaku, only for 4 layers samples, where more diffraction lines of anatase could be identified.

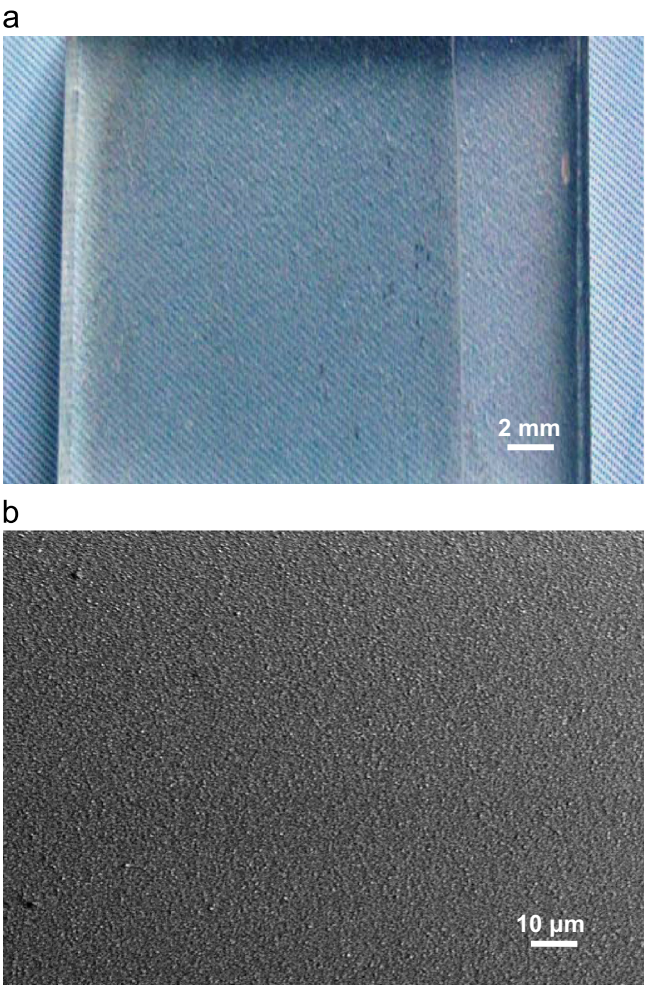

Fig. 3. (a) Optical image of the TiO_2 PEG 20,000 film with three layers and (b) low magnification SEM image in the middle part of the same film.

3.2. SEM and EDX

An optical image of the TiO_2 film doped with PEG 20,000 is shown in Fig. 3a proving the transparency of the film. A low magnification SEM image (Fig. 3b) shows the formation of a continuous film without cracks and highly homogeneous.

The SEM micrograph in Fig. 4a shows the microstructure of the substrate surface, where faceted sub-micron sized crystallites are clearly observed. EDX elemental analysis (Fig. 4c) reveals the presence of Sn and O, corresponding to tin oxide, and Si, from the silica glass support below the tin oxide film. After deposition of the TiO_2 film with PEG, the films are nearly transparent in SEM micrographs (Fig. 4b). The EDX elemental analysis detected only Ti and O in the film, corresponding to TiO_2 (Fig. 4c). The edge-on micrograph of the film (Fig. 4c) reveals an homogeneous thickness, in the sub-micron range and a surface roughness much reduced compared to the faceted SnO_2 substrate.

Fig. 5 compares the microstructure of four layer films, without PEG (Fig. 5a), and with PEG with different molecular weights: 6000 (Fig. 5b), 20,000 (Fig. 5c), and 35,000 (Fig. 5d). The TiO_2 film without PEG does not have microscale porosity (i.e., pores in the scale of 0.1–1 μm) as can be seen in Fig. 5a. The films doped with PEG (Fig. 5b–d) are homogeneous, having similar transparency than those without PEG, and display additional rounded features, with diameters ranging from 20 nm to 400 nm, which correspond to porosity caused by PEG. Additionally, there are some elongated pores, always aligned along the edges of tin oxide crystallites of the substrate. The sample with PEG 6000 has smaller pores, with diameters around 20–80 nm (Fig. 5b), the film doped with PEG 20,000 (Fig. 5c), shows larger pores, with diameters in the range 100–400 nm. We did not observe any rounded pores at the microscale in the samples doped with PEG 35,000 (Fig. 5d); we observed instead in these samples cracked areas with irregular voids, sized a few microns, like the ones shown in Fig. 6, uniformly scattered.

Fig. 6 shows SEM micrographs of the same area of the TiO_2 film doped with PEG 35,000. The secondary electrons image (Fig. 6a) is the topographical view of the film, showing some protruding areas, along with a cracked void. The image is correlated with the back-scattered electrons image of the same region (Fig. 6b), clearly indicating the presence of subsurface cavities (in black) below the protruding areas observed in Fig. 6a. The local micro-cracking of the film doped with PEG 35,000 and the associated voids, such as the one marked by an arrow in Fig. 6a and b, can be explained by the building up of pressure in the subsurface cavities left inside the film due to the combustion of the PEG 35,000 during thermal treatment to 450 °C after deposition. The diameter of the pores induced in the film using PEG 35,000 and the associated microcracking and voids produced after thermal treatment are about one order of magnitude bigger than the film thickness. The observed porosity caused by PEG addition (Table 5) demonstrates the risk of using PEG with high molecular weight (> 20,000) in films of sub-micrometer thicknesses. Therefore we used preferentially PEG 20,000 for further investigations.

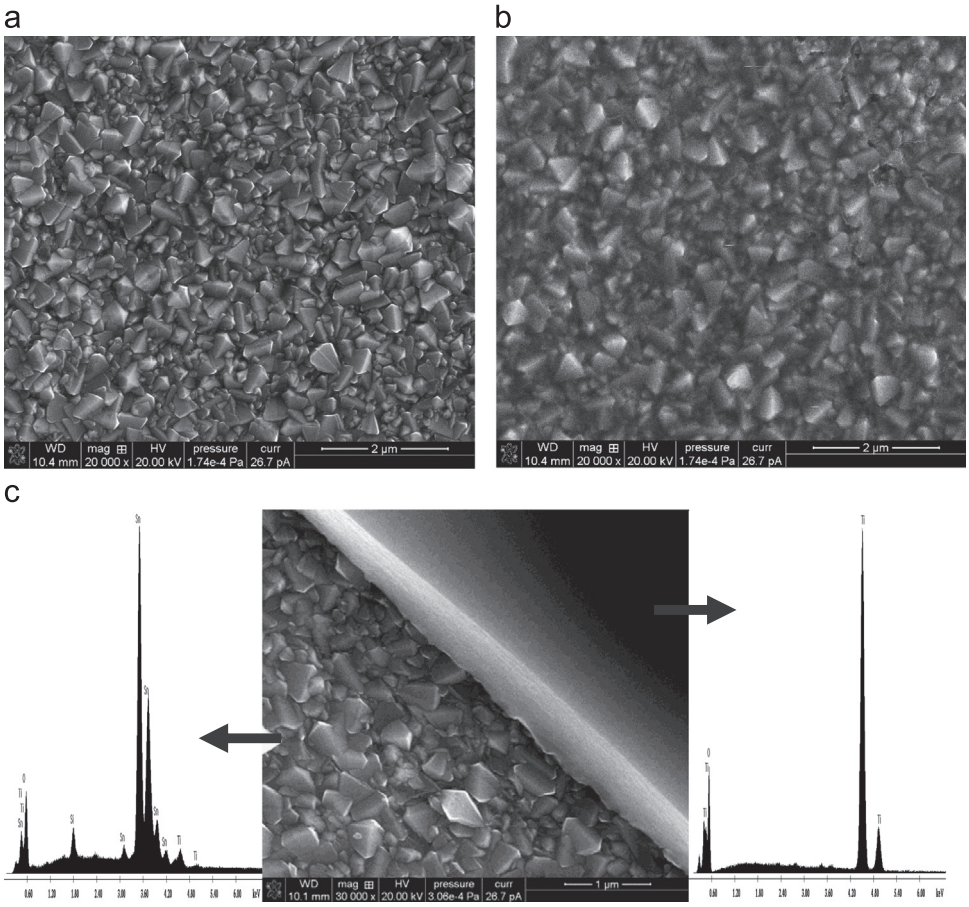

Fig. 4. SEM micrographs and EDX spectra of: (a) FTO substrate; (b) PEG 20,000 doped TiO_2 film and (c) the edge of the this film on the FTO substrate.

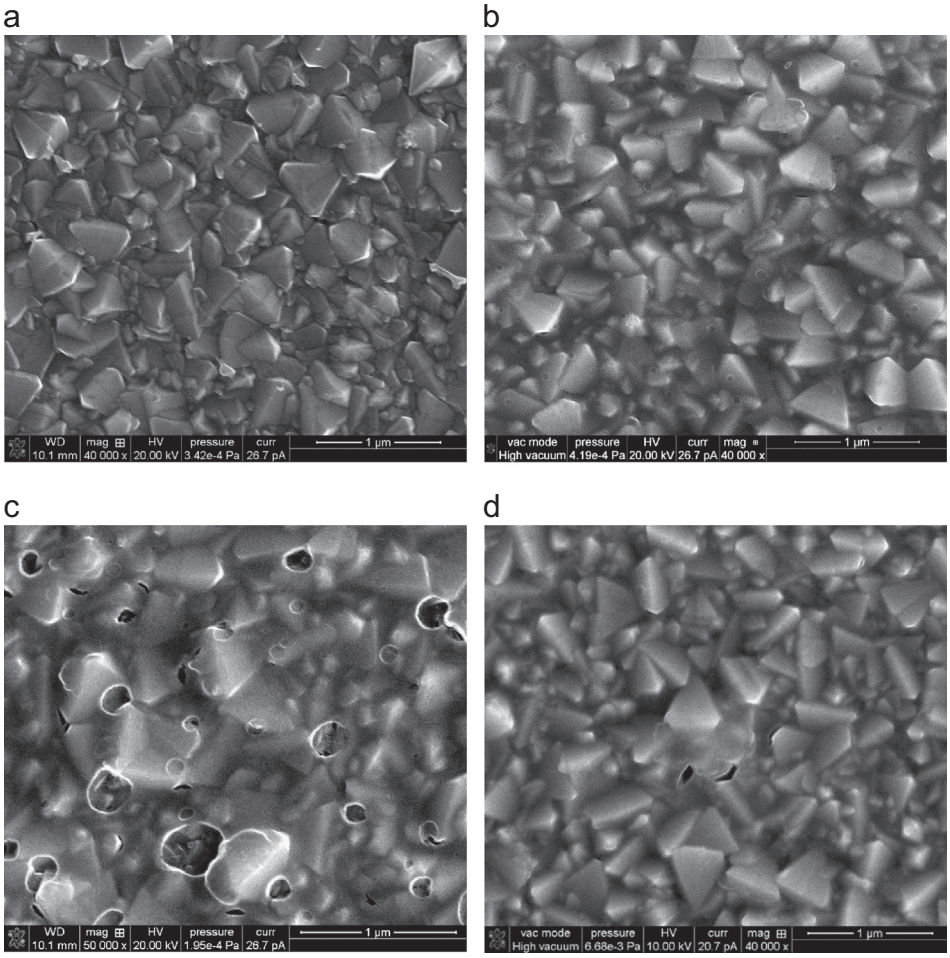

Fig. 5. Comparison between SEM micrographs of the TiO_2 films with one layer: (a)-undoped; (b) doped with PEG 6000; (c) doped with PEG 20,000 and (d) doped with PEG 35,000.

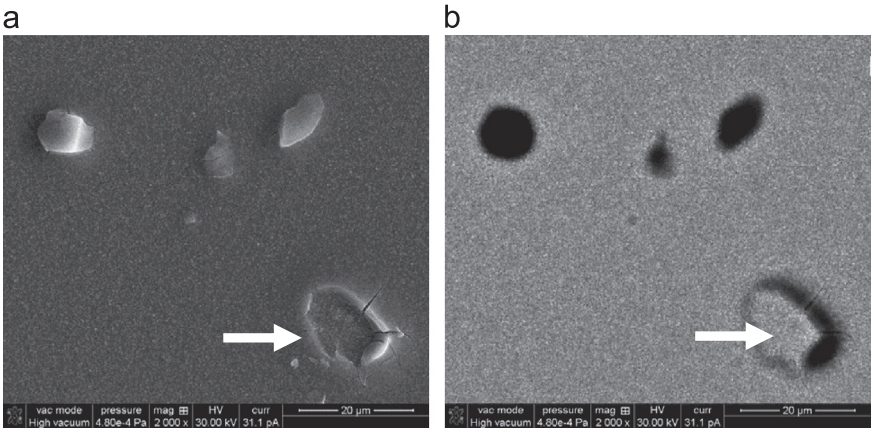

Fig. 6. SEM micrographs of the TiO_2 film with one layer doped with PEG 35,000, (a) secondary electrons and (b) back-scattered electrons, showing the presence of sub-surface cavities.

Detailed SEM measurements at higher magnification (Fig. 7) reveal the particle size granulation of the TiO_2 films at the surface, with grain size features ~10–20 nm in agreement with grain sizes calculated from XRD.

SEM images of the 3 layers TiO_2 film doped with PEG 20,000 (Fig. 8a) show a lower transparency of the film to the electron beam, in comparison with the images in Fig. 5a–d, a clear indication that the film is thicker. The edge-on micrograph taken

on a piece broken from the TiO_2 film (Fig. 8b) allows observing clearly the film section, showing that pores are preferentially located at the outer surface of the film.

3.3. AFM

A detailed morphology analysis was obtained by AFM at the scale of 8 μm × 8 μm (Fig. 9). The FTO substrate has a morphology consisting of large SnO_2 grains (large crystallites with sharp edges as presented in Fig. 4a) leading to high RMS roughness values of up to 36 nm. Qualitatively it can be seen that the TiO_2 film covers completely the crystallites of substrate (visible as less shaper crystallite edges after TiO_2 deposition) while quantitatively is accompanied by a decrease in roughness from 36 nm (on the substrate) down to 20–26 nm for the as-prepared first layer. After the annealing at 450 °C, the TiO_2 – PEG film is characterized by an increase in roughness. This can be due to the stress induced by the PEG removal from the one layer film matrix, which is not observed at TiO_2 film without PEG.

Further on, adding more layers (including successive thermal treatments) the films become slightly thicker (see SE results below) and the roughness decreases (Fig. 10) so that the RMS values are almost bunched for the films with 2 layers, while with 4 layers the lowest RMS values (around 12 nm) are obtained.

This behavior is expected due to the fact that the existing pores after the PEG elimination (burned out after TT) are filled up at the second deposition, and thus the roughness decreases successively up to 4 layers deposition.

Table 5
The variation of pore diameter versus PEG molecular weight.

PEG mol. weight	Pore diameter
0	No pores
6000	20–80 nm
20,000	100–400 nm
35,000	> 600–800 nm

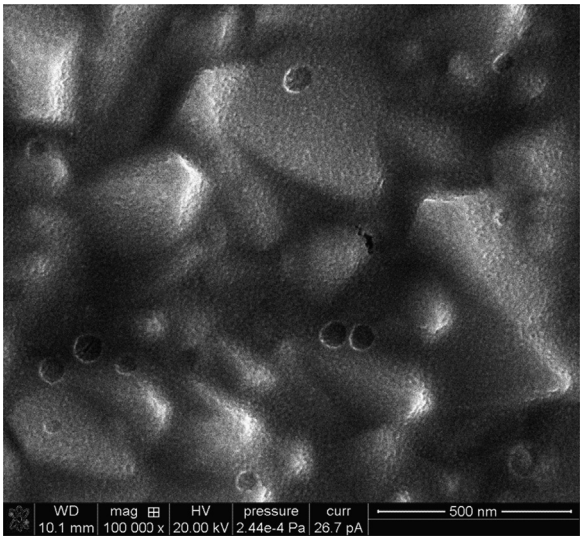

Fig. 7. SEM micrograph of the 1 layer TiO_2 film doped with PEG 20,000, showing its surface roughness associated to TiO_2 grain size.

3.4. SE

The influence of the PEG on the optical properties of TiO_2 layer was studied by Spectroscopic Ellipsometry.

Firstly, the substrate was measured at 70° angle of incidence and fitted by a two-layer model (surface roughness layer/SnO_2:F layer/soda lime glass)–Fig. 11a. The SnO_2:F film was modeled using Drude and Lorentz oscillators [40] and the roughness layer with the effective medium approximation [41], considering 50% voids and 50% SnO_2:F. From the best fit, the thickness (~715 nm) and the dielectric functions of the fluorine doped tin oxide (SnO_2:F) were obtained (Fig. 11b), in agreement with the results obtained by Akagawa and Fujiwara [42].

A four-layer model (surface roughness layer/TiO_2 film/interface layer/SnO_2:F layer/soda lime glass) was used to fit the ellipsometric spectra concerning the TiO_2 – PEG films deposited on TCO30–8 substrate – Fig. 12a. The interface layer (between substrate and TiO_2 film) was suggested by the SEM micrograph in Fig. 4a which shows the microstructure of the surface of the fluorine doped tin oxide (SnO_2:F) layer, where sub-micron sized crystallites are clearly observed. The interface layer was modeled by the

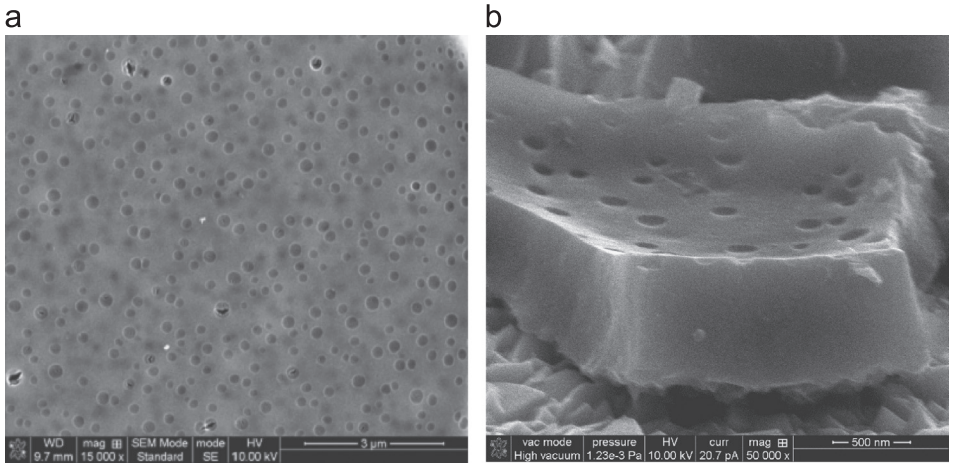

Fig. 8. SEM micrograph of 3 layer TiO_2 film: (a) measured at the edge of the sample and (b) the view of the edge of a piece broken from the TiO_2 film.

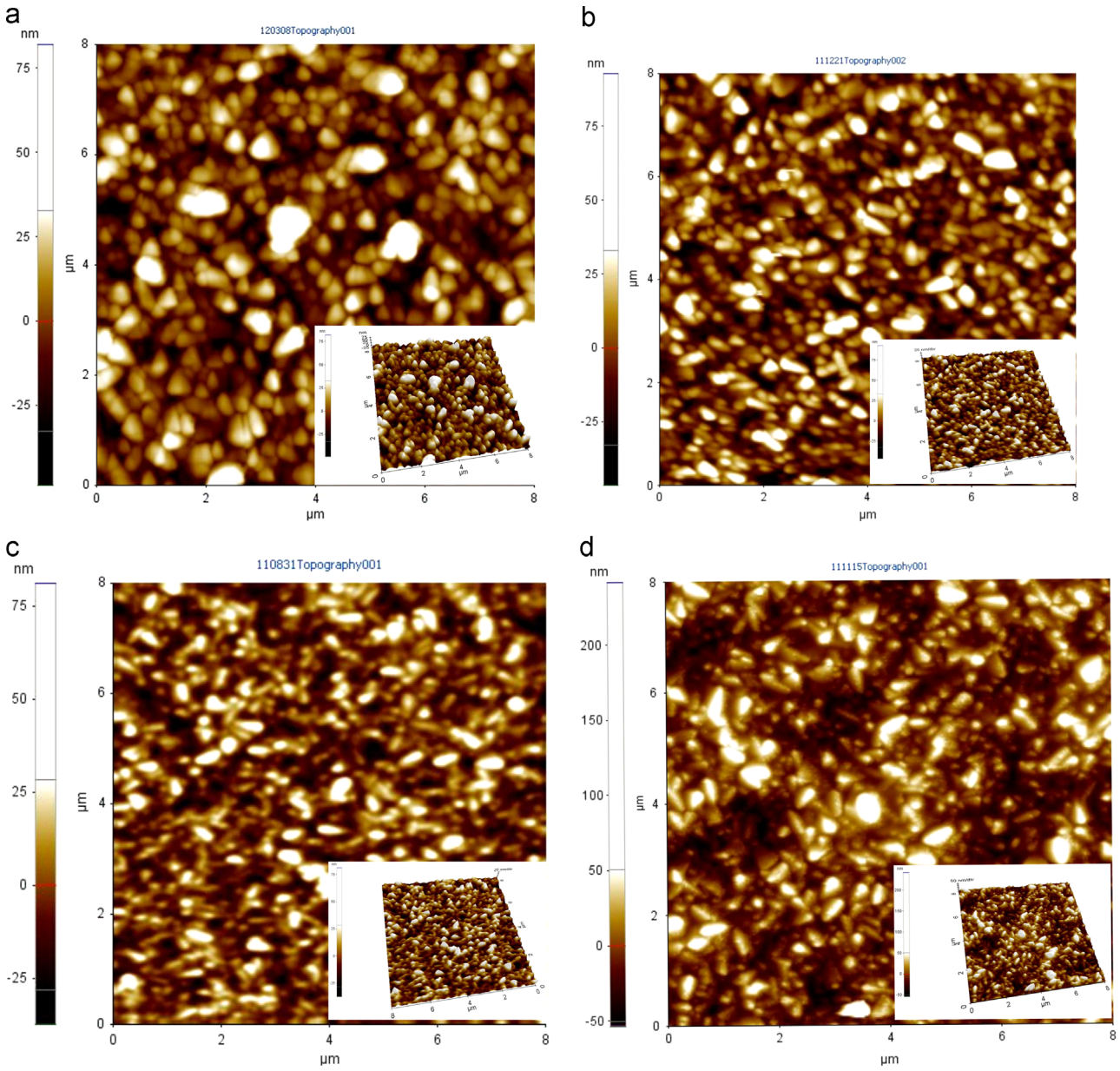

Fig. 9. 2D AFM topographic images (inset 3D) at the scale of (8 µm × 8 µm) for the TiO_2-PEG films with 3 layers: (a) without PEG, (b) PEG 6000, (c) PEG 20,000 and (d) PEG 35,000.

"intermix" option in the WVASE32® program [40], which is treated as a mixed layer composed of the upper and lower lying materials with 50% – 50% volume fractions on basis of effective medium approximation [41], with the thickness being the only free parameter. The thickness of the interface layer was found to depend on the PEG molecular weights (as an example, for the film studied by SEM in Fig. 4a, the intermix layer thickness calculated by SE is 53 ± 1 nm, in good agreement with the value estimated by SEM). To model the TiO_2 layer, the Cauchy equation was used. The film roughness layer was modeled, as in the case of the substrate roughness, with the Effective Medium Approximation (EMA) model [41] with fix percentage: 50% voids and 50% TiO_2. From the best fit (one example is illustrated for TiO_2-PEG 20.000 film with 4 layers in Fig. 12b) the thickness and the refractive index were obtained.

For all samples the thickness of TiO_2 layer decreases (Fig. 13a) after the first thermal treatment when the film is densified due to the PEG leaving from the system and then increases after each new deposition (a new deposition is followed by a new thermal treatment). The increase of thickness observed for the films with 2–4 layers is relatively small; this may be related to the filling of existing pores formed by PEG elimination during the first TT.

The porosity of the films were calculated with the formula [43] $P = 1 - (n^2 - 1)/(n_A^2 - 1)$, where $n_A = 2.52$ is the refractive index of anatase (at $\lambda = 550$ nm) and n is the refractive index of PEG doped TiO_2 film at the same wavelength (Fig. 13b).

After two layer depositions (and two TT) the porosities are similar for all films with and without PEG addition, because PEG is eliminated after TT at 450 °C. This result is sustained from the previous literature data [44,45], that underlined the

depolymerization of the PEG during the reactions in solution and also by thermal treatment.

There are two kinds of porosity in the films: intrinsic and extrinsic. The intrinsic one is related with the preparation method and is formed by small mesopores of similar size than crystallite size (~10 nm) [32]. SEM analysis of the films can determine only the extrinsic porosity caused by PEG addition. The ellipsometric analysis can determine the total porosity. The results indicate that only the one-layer films show significant extrinsic porosity caused by PEG, subsequent layer deposition and thermal treatments after the first layer leading to the densification of the film and the disappearance of most of the extrinsic porosity, explaining why the porosity diminishes after the deposition of the second layer. SEM observations of the films cross section (Fig. 8b) confirmed that in multilayer films extrinsic porosity remains located mostly at the outer layer of the film.

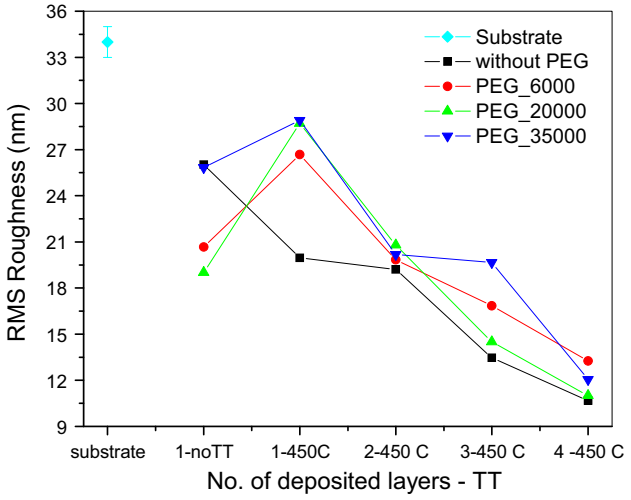

Fig. 10. Superimposed RMS roughness behaviors vs. number of deposited layers.

3.5. Transmission

The transmission measurements performed by ellipsometry (Fig. 14a) showed that introducing PEG during film preparation leads to a higher transmittance than that of undoped film and even of FTO substrate, being a promising TCO material for solar cell applications.

The evolution of transmission with the number of deposited layers is presented in Fig. 14b. It can be seen that the transmittance increases with the number of depositions and

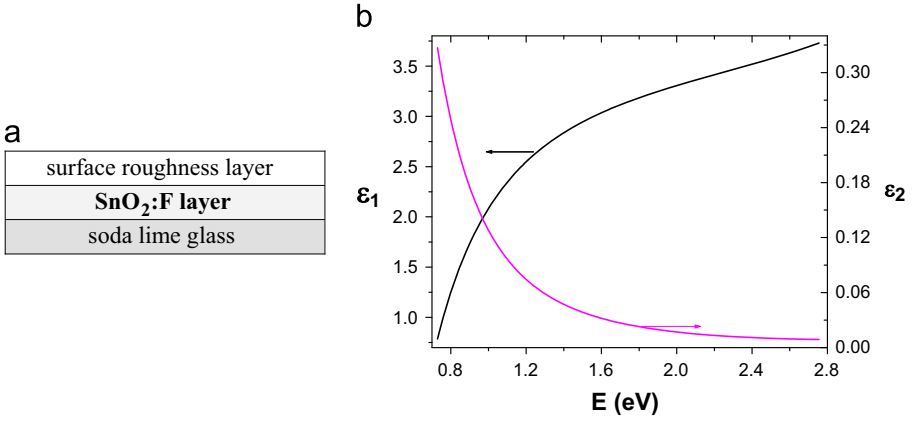

Fig. 11. (a) Model used to fit the experimental SE spectra of the substrate material (TCO30-8 type) and (b) dielectric functions of the fluorine doped tin oxide (SnO_2:F) layer.

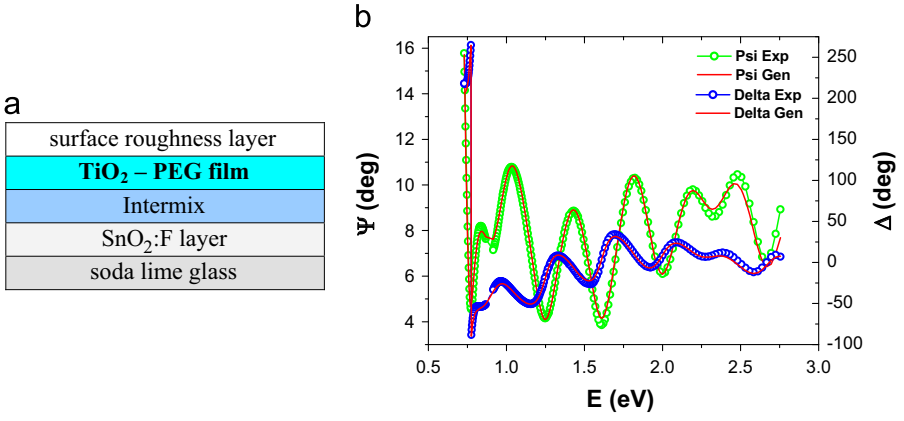

Fig. 12. (a) Model used to fit the experimental SE spectra of the TiO_2 – PEG films and (b) superimposed experimental and generated Ψ and Δ ellipsometric data of the TiO_2 – PEG 20,000 films with 4 layers.

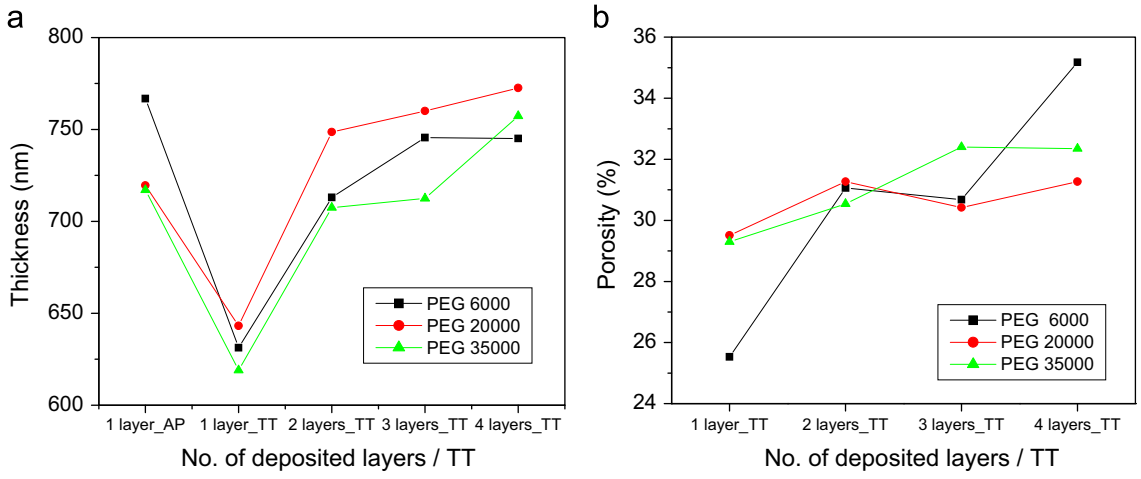

Fig. 13. Thickness (a) and porosity (b) determined from ellipsometric measurements for the TiO_2 – PEG films.

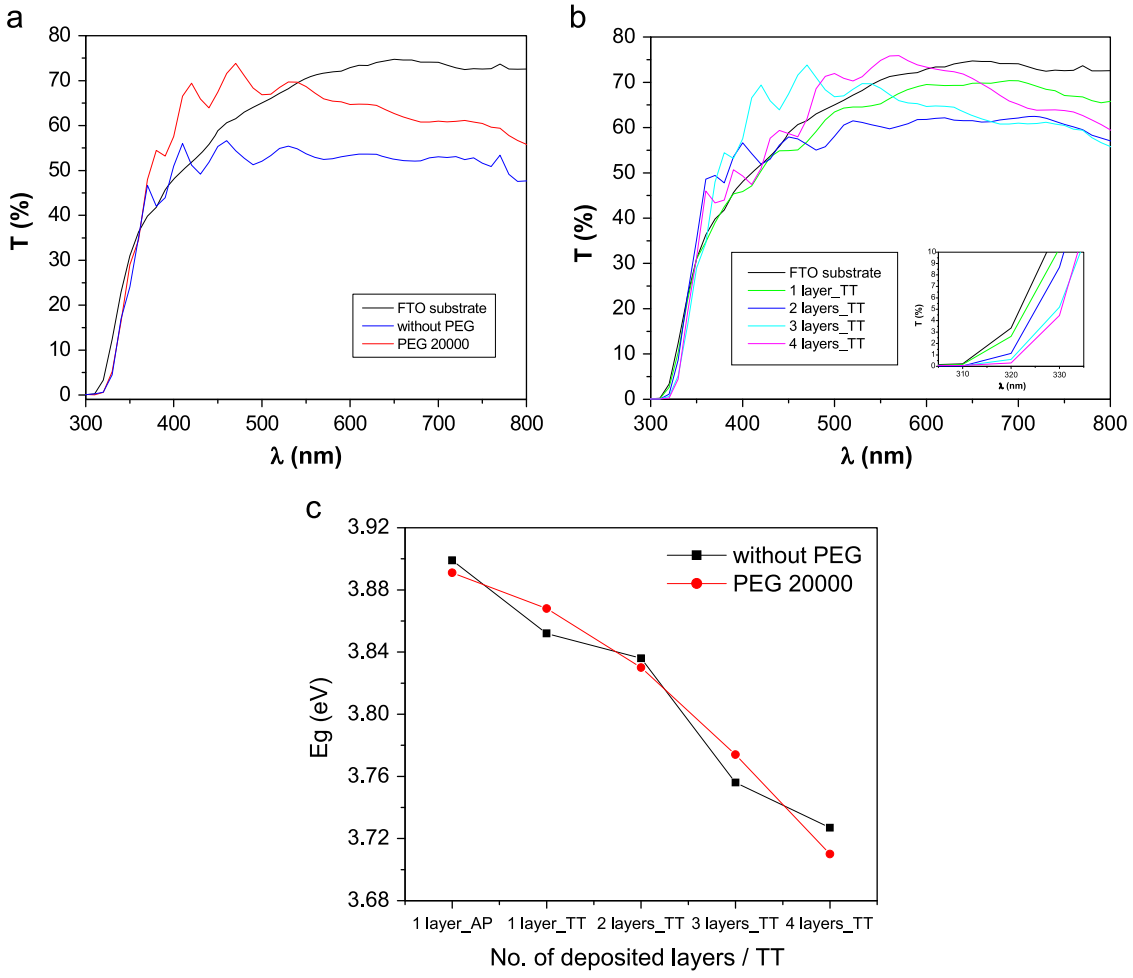

Fig. 14. (a) Transmission of 3 layer undoped and PEG 20,000 dopped TiO_2 films in comparison with the bare FTO substrate; (b) Change of transmission spectra of TiO_2 films doped with PEG 20,000 with number of depositions (insertion presents details about absorption edge spectra) and (c) band gap energy (E_g) variation with number of depositions for the undoped and PEG 20,000-doped TiO_2 films.

the maximum transmittance value shifted to higher wavelengths. As for example for one layer TT film the transmission is maximum (69%) in the 600–700 nm range and for four layer films is maximum (76%) at around of 560 nm range. Fig. 14c presents the direct optical band gap calculated from transmission curves [46]. The absorption edge is also shifting almost linearly to longer wavelengths with the deposition number as could be observed from Fig. 14c.

4. Conclusions

The properties of sol–gel multilayered (1–4) films were studied in function of PEG molecular weight introduced in the TiO_2 matrix.

XRD and SEM proved that after annealing all films (with and without PEG) crystallize in the anatase phase (even single layer films). The crystallization quality is improved increasing the number of layer depositions and the crystallite size decreases when PEG is introduced in the matrix.

TiO_2 sol–gel films have an intrinsic porosity due to the preparation method and the addition of PEG leads to an extrinsic one, which pore size is determined by PEG molecular weight. The extrinsic porosity is very significant after first layer deposition. SE measurements have shown that the total porosity (intrinsic and extrinsic) has similar values for all doped films after the deposition of a second layer, no matter the molecular weight of the PEG used, due to the densification of the films, that confines extrinsic porosity to the film outer surface.

The films with PEG have large porosities (showed by SEM and SE) which could be useful for biomedical applications, such as embedding of drugs or dye sensitized solar cell.

Adding of PEG during TiO_2 films preparation and increasing the number of depositions leads to higher values of transmittance.

Acknowledgment

This work was supported by the Romanian PN-II-ID-PCE-2011-3-0446 and Romanian National Agency of Scientific Research through contract no 274/2010 – "Novocell".

Support of the EU (ERDF) and Romanian Government, that allowed for acquisition of the research infrastructure under POS-CCE O 2.2.1 project INFRANANOCHEM – No. 19/01.03.2009, is gratefully acknowledged.

References

[1] B. O'Regan, M. Gratzel, A low-cost, high-efficiency solar cell based on dyesensitized colloidal TiO_2 films, Nature 353 (1991) 737–740.

[2] A. Zaban, O.I. Micic, B.A. Gregg, A.J. Nozik, Photosensitization of nanoporous TiO_2 electrodes with InP quantum dots, Langmuir 14 (1998) 3153–3156.

[3] R. Argazzi, C.A. Bignozzi, T.A. Heimer, F.N. Castellano, G.J. Meyer, Lightinduced charge separation across Ru(II)–modified nanocrystalline TiO_2 interfaces with phenothiazin donors, Journal of Physical Chemistry 101 (1997) 2591–2597.

[4] H. Deng, Z. Lu, H. Mao, H. Xu, The liquid junction cell based on the nanostructured TiO_2 electrode sensitized with zinc tetrasulfonated phthalocyanine, Chemical Physics 221 (1997) 323–331.

[5] S. Cosnier, A. Senillou, M. Gratzel, P. Comte, N. Vlachopoulos, N. J. Renault, C. Martelet, A glucose biosensor based on enzyme entrapment within polypyrrole films electrodeposited on mesoporous titanium dioxide, Journal of Electroanalitical Chemistry 469 (1999) 176–181.

[6] C. Trapalis, M. Gartner, M. Modreanu, G. Kordas, M. Anastasescu, R. Scurtu, M. Zaharescu, Stabilization of the anatase phase in $TiO_2(Fe^{3+}$, PEG) nanostructured coatings, Applied Surface Science 253 (2006) 367–371.

[7] W. Sun, S. Zhang, Z. Liu, C. Wang, Z. Mao, Studies on the enhanced photocatalytic hydrogen evolution over Pt/PEG-modified TiO_2 photocatalysts, International Journal of Hydrogen Energy 33 (2008) 1112–1117.

[8] L.C.-K. Liau, H. Chang, T.C.-K. Yang, C.-L. Huang, Effect of poly (ethyleneglycol) additives on the photocatalytic activity of TiO_2 films prepared by sol–gel processing and low temperature treatments, Journal of the Chinese Institute of Chemical Engineers 39 (2008) 237–242.

[9] N. Negishi, F. He, S. Matsuzawa, K. Takeuchi, K. Ohno, Wave-guide type photoreactor for water purification, Comptes Rendus Chimie 9 (5–6) (2006) 822–828.

[10] H. Gao, M. Sänger, R. Luginbühl, H. Sigrist, Immunosensing with photoimmobilized immunoreagents on planar optical wave guides, Biosensors and Bioelectronics 10 (3–4) (1995) 317–328.

[11] J.-C. Woo, Y.-S. Chun, Y.-H. Joo, C.-I. Kim, The dry etching property of TiO_2 thin films using metal-insulator-metal capacitor in inductively coupled plasma system, Vacuum 86 (12) (2012) 2152–2157.

[12] D. Rathee, M. Kumar, S.K. Arya, Deposition of nanocrystalline thin TiO_2 films for MOS capacitors using sol–gel spin method with Pt and Al top electrodes, Solid-State Electronics 76 (2012) 71–76.

[13] T. Zhu, Y. Lin, Y. Luo, X. Hu, W. Lin, P. Yu, C. Huang, Preparation and characterization of TiO_2-regenerated cellulose inorganic–polymer hybrid membranes for dehydration of caprolactam, Carbohydrate Polymers 87 (1) (2012) 901–909.

[14] Y. Yang, H. Zhang, P. Wang, Q. Zheng, J. Li, The influence of nanosized TiO_2 fillers on the morphologies and properties of PSF UF membrane, Journal of Membrane Science 288 (1–2) (2007) 231–238.

[15] N.N. Dinh, N.M. Quyen, D.N Chung, M. Zikova, V-V. Truong, Highly-efficient electrochromic performance of nanostructured TiO_2 films made by doctor blade technique, Solar Energy Materials and Solar Cells 95 (2) (2011) 618–623.

[16] F. Campus, P. Bonhôte, M. Grätzel, S. Heinen, L. Walder, Electrochromic devices based on surface-modified nanocrystalline TiO_2 thin-film electrodes, Solar Energy Materials and Solar Cells 56 (3–4) (1999) 281–297.

[17] Q. Zhou, Y. Huang, G. Xie, Investigation of the applicability of highly ordered TiO_2 nanotube array for enrichment and determination of polychlorinated biphenyls at trace level in environmental water samples, Journal of Chromatography A 1237 (2012) 24–29.

[18] G. Boulousis, K. Tsougeni, K. Ellinas, A. Speliotis, A. Tserepi, E. Gogolides, TiO_2 affinity chromatography microcolumn on Si substrates for phosphopeptide analysis, Procedia Engineering 25 (2011) 717–720.

[19] S. Xu, M. Zheng, X. Zhang, J. Zhang, Y.-I. Lee, Nano TiO_2-based preconcentration for the speciation analysis of inorganic selenium by using ion chromatography with conductivity detection, Microchemical Journal 101 (2012) 70–74.

[20] K.-M. Lee, C.-Y. Hsu, W.-H. Chiu, M.-C. Tsui, Y.-L. Tung, S.-Y. Tsai, K.-C. Ho, Dye-sensitized solar cells with a micro-porous TiO_2 electrode and gel polymer electrolytes prepared by in situ cross-link reaction, Solar Energy Materials and Solar Cells 93 (11) (2009) 2003–2007.

[21] H. Park, W.-R. Kim, H.-T. Jeong, J.-J. Lee, H.-G. Kim, W.-Y. Choi, Fabrication of dye-sensitized solar cells by transplanting highly ordered TiO_2 nanotube arrays, Solar Energy Materials and Solar Cells 95 (1) (2011) 184–189.

[22] J.-A. Jeong, H.-K. Kim, Thickness effect of RF sputtered TiO_2 passivating layer on the performance of dye-sensitized solar cells, Solar Energy Materials and Solar Cells 95 (1) (2011) 344–348.

[23] E. Stathatos, Y. Chen, D.D. Dionysiou, Quasi-solid-state dye-sensitized solar cells employing nanocrystalline TiO_2 films made at low temperature, Solar Energy Materials and Solar Cells 92 (11) (2008) 1358–1365.

[24] M.DJ. Blesic, Z.V. Saponjic, J.M. Nedeljkovic, D.P. Uskokovic, TiO_2 films prepared by ultrasonic spray pyrolysis of nanosize precursor, Materials Letters 54 (2002) 298–302.

[25] C.H. Heo, S.-B. Lee, J.-H. Boo, Deposition of TiO_2 thin films using RF magnetron sputtering method and study of their surface characteristics, Thin Solid Films 475 (2005) 183–188.

[26] J.-Y. Lee, W.Y. Lee, D.-K. Choi, J. Oh, Structure and properties of Co doped TiO_2 thin films on Si(100) by pulsed laser deposition method, Journal of Ceramic Processing Research 7 (1) (2006) 58–61.

[27] A.A. Hateef, B.D. Balawa, A.F. Saleh, M.W. Mahmmod, Effect of the thickness on electrical properties of TiO_2 thin films prepared by thermal

chemical spray pyrolysis deposition, International Research Journal of Engineering Science, Technology and Innovation 1 (6) (2012) 175–179.
[28] H. Sun, C. Wang, S. Pang, X. Li, Y. Tang, M. Liu, Photocatalytic TiO_2 films prepared by chemical vapor deposition at atmosphere pressure, Journal of Non-Crystalline Solids 354 (2008) 1440–1443.
[29] B. Guo, Z. Liu, L. Hong, H. Jiang, J.Y. Lee, Photocatalytic effect of the sol–gel derived nanoporous TiO_2 transparent thin films, Thin Solid Films 479 (2005) 310–315.
[30] R. Mechiakh, R. Bensaha, Analysis of optical and structural properties of sol-gel TiO_2 thin films, Moroccan Journal of Condensed Matter 7 (1) (2006) 54–57.
[31] B. Guo, Z. Liu, L. Hong, H. Jiang, Sol gel derived photocatalytic porous TiO_2 thin films, Surface and Coatings Technology 198 (2005) 24–29.
[32] M. Zaharescu, M. Crisan, L. Simionescu, D. Crişan, M. Gartner, TiO_2-based porous materials obtained from gels in different experimental conditions, Journal of Sol–Gel Science and Technology 8 (1997) 249–253.
[33] M. Zaharescu, M. Crisan, I. Musevic, Atomic force microscopy study of TiO_2 films obtained by sol–gel method, Journal of Sol–Gel Science and Technology 13 (1998) 769–773.
[34] S. Bu, Z. Jin, X. Liu, L. Yang, Z. Cheng, Fabrication of TiO_2 porous thin films using peg templates and chemistry of the process, Materials Chemistry and Physics 88 (2004) 273–279.
[35] M. Gartner, C. Trapalis, N. Todorova, T. Giannakopoulou, G. Dobrescu, M. Anastasescu, P. Osiceanu, A. Ghita, M. Enache, L. Dumitru, T. Stoica, M. Zaharescu, J.Y. Bae, S.H. Suh, Doped sol–gel TiO_2 films for biological applications, Bulletin of the Korean Chemical Society 29 (5) (2008) 1038–1042.
[36] R.S. Sonawane, B.B. Kale, M.K. Dongare, Preparation and photocatalytic activity of Fe–TiO_2 thin films prepared by sol–gel dip coating, Materials Chemistry and Physics 85 (2004) 52–57.
[37] M. Crisan, M. Zaharescu, D. Crisan, R. Ion, M. Mihalache, Vanadium doped solgel TiO_2 coatings, Journal of Sol–Gel Science and Technology 13 (1998) 775–778.
[38] C. Trapalis, P. Keivanidis, G. Kordas, M. Zaharescu, M. Crisan, A. Szatvany, M. Gartner, $TiO_2(Fe^{3+})$ nanostructurated thin films with antibacterial properties, Thin Solids Films 433 (1–2) (2003) 186–190.
[39] A. Barau, M. Crisan, M. Gartner, A. Jitianu, M. Zaharescu, A. Ghita, V. Danciu, V. Cosoveanu, I.O. Marian, Phototermal and photocatalytic processes on TiO_2 based materials prepared by sol–gel method, Journal of Sol–Gel Science and Technology 37 (2006) 175–178.
[40] H.G. Tompkins, WVASE32® Software Training Manual, J.A. Woollam Co., Inc., Lincoln, NE, USA, 2006.
[41] D.A.G Bruggeman, Berechnung verschiedener physikalischer Konstanten von heterogenen Substanzen, Annalen der Physik 24 (1935) 636–679.
[42] M. Akagawa, H. Fujiwara, High-precission characterization of textured a-Si:H/SnO_2:F structures by spectroscopic ellipsometry, Journal of Applied Physics 110 (2011) 073518-1–073518-9.
[43] M.M. Hasan, A.S.M.A. Haseeb, R. Saidur, H.H. Masjuki, Effects of annealing treatment on optical properties of anatase TiO_2 thin films, International Journal of Chemical and Biological Engineering 1 (2) (2008) 92–96.
[44] S. Han, C. Kim, D. Kwon, Thermal/oxidative degradation and stabilization of polyethylene glycol, Polymer 38 (1997) 317–323.
[45] M. Ito, K. Nagai, Degradation issues of polymer materials used in railway field, Polymer Degradation and Stability 93 (2008) 1723–1735.
[46] R. Lopez, R. Gomez, Band gap energy estimation from diffuse reflectance measurements on sol–gel and commercial TiO_2: a comparative study, Journal of Sol–Gel Science and Technology 61 (2012) 1–7.